City Research Online

City St George's, University of London

Citation: Karim, M. R., Ahmad, H. & Rahman, B. M. (2017). All-Normal-Dispersion Chalcogenide Waveguides for Ultraflat Supercontinuum Generation in the Mid-Infrared Region. IEEE Journal of Quantum Electronics, 53(2), pp. 1-6. doi: 10.1109/jqe.2017.2677380

This is the accepted version of the paper.

This version of the publication may differ from the final published version. To cite this item please consult the publisher's version.

Permanent repository link: https://openaccess.city.ac.uk/id/eprint/18499/

Link to published version: https://doi.org/10.1109/jqe.2017.2677380

Copyright and Reuse: Copyright and Moral Rights remain with the author(s) and/or copyright holders. Copies of full items can be used for personal research or study, educational, or not-for-profit purposes without prior permission or charge, unless otherwise indicated, provided that the authors, title and full bibliographic details are credited, a hyperlink and/or URL is given for the original metadata page and the content is not changed in any way. For full details of reuse please refer to City Research Online policy.

City Research Online: http://openaccess.city.ac.uk/ publications@citystgeorges.ac.uk

All-Normal-Dispersion Chalcogenide Waveguides for Ultraflat Supercontinuum Generation in the Mid-Infrared Region

***Abstract*—We show numerically how a chalcogenide planar waveguide designed to exhibit normal dispersion over a wide spectral range around the pump wavelength can produce relatively flat supercontinuum in the mid-infrared regime. A 1-cm-long channel waveguide, made using $Ge_{11.5}As_{24}Se_{64.5}$ glass and pumped at 1.55 μm using short optical pulses with only 25 W peak power, produced a supercontinuum that was nearly 600 nm wide. Employing the same pump source with a peak power of 100 W, the supercontinuum could be extended to beyond 2.2 μm with a bandwidth of 1000 nm. By shifting the pump wavelength to 3.1 μm and using pulses with peak powers of up to 3 kW, the resulting ultraflat supercontinuum extended from 2 to 5.5 μm. Even a wider spectral range (1.8–6 μm) can be realized if MgF_2 glass is used for the lower cladding while maintaining power variations below 5 dB over the entire bandwidth.**

***Index Terms*—Numerical analysis and approximation, Nonlinear optics, Dispersion, Chalcogenide, Channel waveguide, Supercontinuum generation.**

I. Introduction

Supercontinuum (SC) generation has attracted considerable attention in recent years because of its diverse applications that include biomedical imaging and high-precision measurements [1]–[3]. Broadband SC is usually generated by pumping optimized optical waveguides with ultrashort pulses in the anomalous dispersion region. The physical process of soliton fission and subsequent spectral evolution is well understood by now [3]. However, this approach is sensitive to pump-pulse fluctuations and produces SC spectra that are only partially coherent over the entire SC bandwidth [4].

One approach to obtain coherent SC spectra is to pump the optical waveguides such that pulses experience normal dispersion throughout their evolution. Since pulses do not propagate as solitons, it becomes possible to produce SC spectra with high coherence and high spectral flatness [5]. Although optical pulse evolution in a normally dispersive waveguide leads to a relatively narrower spectra than anomalous dispersion regime, comparatively smooth and flat spectra can be observed through the suppression of soliton fission under the same operating condition [6]. A number of numerical and experimental investigations have shown that SC spectra extending from ultraviolet to near-infrared can be generated using normally dispersive photonic crystal fibers made with silica glass [6]–[10]. Relatively high loss of silica glass beyond 1.7 μm limits its use for SC generation in the mid-infrared region [11]. The loss problem can be solved using fibers made with chalcogenide (ChG) glass [12]. Indeed, photonic crystal fibers made with ChG glass and exhibiting normal dispersion have been used for SC generation in the mid-infrared region [13], [14].

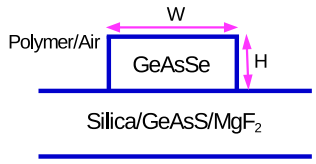

Fig. 1: Channel waveguide geometry

Recently interest has grown in using ChG-glass planar waveguides (as an alternative to ChG fibers) for mid-infrared SC generation. Several experiments have used such waveguides with a suitably tailored group-velocity dispersion (GVD) such that the zero-dispersion wavelength is close to the central wavelength of input pump pulses [15]–[17]. However, to generate coherent ultraflat SC spectra, the ChG planar waveguide needs to be engineered in such a way that the GVD value of the optimized waveguide at the pump wavelength lies in the normal-dispersion region, is relatively small in magnitude at this wavelength, and increases on both sides of it. In this paper, we discuss how ChG waveguides can be designed to meet this objective and numerically predict that they can produce octave-spanning mid-infrared region SC that is both coherent and relatively flat over its entire bandwidth.

II. Numerical Model

The cross-section of the our proposed channel waveguide is shown in Fig. 1. Its core is made of the $Ge_{11.5}As_{24}Se_{64.5}$ glass with either an inorganic polymer glass (IPG) whose refractive index value of 1.51 or air acting as upper cladding. For the lower cladding we consider three different materials: silica, $Ge_{11.5}As_{24}S_{64.5}$, or MgF_2 glass. We optimize our waveguides for pumping at two different wavelengths, namely 1.55 μm or 3.1 μm. The wavelength dependence of the GVD is quite sensitive to the both the width W and height H of the core region of the waveguide. We vary both of them using a numerical code based on the full-vectorial finite-element method [21]. For a specific value of W and H the mode solver provides us with the propagation constant of the fundamental mode as a function of optical frequency, which is used to calculate the GVD as a function of wavelength.

To study the formation of SC by launching short optical pulses in the normal dispersion regime of our optimized ChG waveguide, we solve the widely used generalized nonlinear

Schrödinger equation [1]–[3] that also includes the two-photon absorption that cannot be neglected for ChG glasses [18]:

$$\frac{\partial}{\partial z}A(z,T) = -\frac{\alpha}{2}A + \sum_{m\geq 2}^{10}\frac{i^{m+1}}{m!}\beta_m\frac{\partial^m A}{\partial T^m} + i\left(\gamma + i\frac{\alpha_2}{2A_{\text{eff}}}\right)\left(1+\frac{i}{\omega_0}\frac{\partial}{\partial T}\right) \times \left(A(z,T)\int_{-\infty}^{\infty} R(T)\mid A(z,T-T')\mid^2 dT'\right), \quad (1)$$

Here $A(z,T)$ is the electric-field envelope in a retarded frame moving at the group velocity $1/\beta_1$ ($T = t - \beta_1 z$), β_m ($m \geq 2$) is the mth-order dispersion parameter, and ω_0 is the pump frequency. The nonlinear coefficient is defined as $\gamma = n_2\omega_0/(cA_{\text{eff}})$, where n_2 is the nonlinear refractive index, c is the speed of light in vacuum, and A_{eff} is the effective mode area at the pump frequency. Linear losses are included through α and nonlinear loss is included through $\alpha_2 = 9.3 \times 10^{-14}$ m/W, representing the two-photon absorption coefficient [19].

Intrapulse Raman scattering plays an important role in the process of SC generation [3]. It is included through a response function

$$R(t) = (1 - f_R)\delta(t) + f_R h_R(t), \quad (2)$$

that includes both the Kerr and Raman contributions, the later

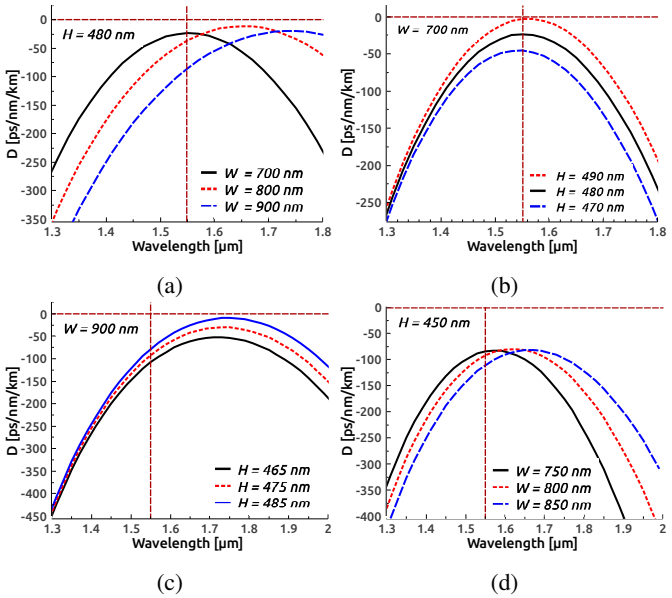

Fig. 2: GVD curves of ChG waveguides pumped at 1.55 μm when W is varied with H constant in (a) and (d) and H is varied with W constant in (b) and (c). Vertical dashed line indicates pump wavelength.

having the form

$$h_R(t) = \frac{\tau_1^2 + \tau_2^2}{\tau_1\tau_2^2}\exp\left(-\frac{t}{\tau_2}\right)\sin\left(\frac{t}{\tau_1}\right), \quad (3)$$

where the parameters for the ChG glass are $f_R = 0.148$, $\tau_1 = 23$ fs, and $\tau_2 = 164.5$ fs [13].

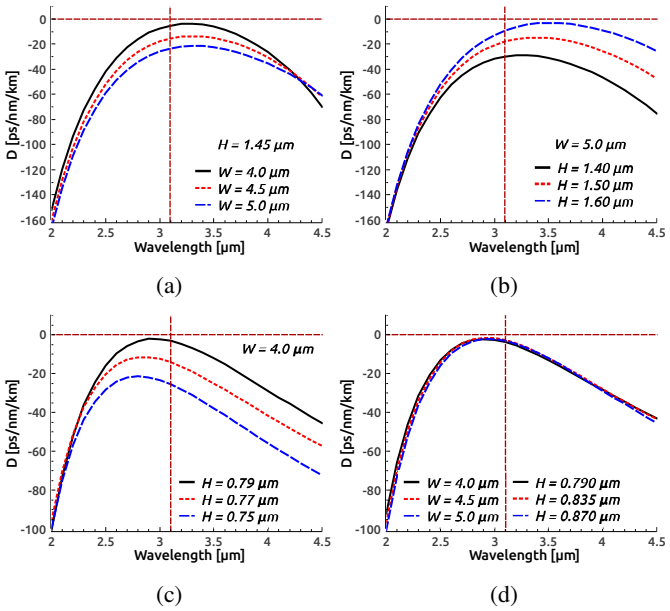

Fig. 3: GVD curves of ChG waveguides pumped at 3.1 μm for several choices of W and H. Lower cladding layer is made of $Ge_{11.5}As_{24}S_{64.5}$ in (a) and (b) and of MgF_2 in (c) and (d). Vertical dashed line indicates pump wavelength.

III. Dispersion Engineering

As mentioned earlier, we want to design channel waveguides exhibiting normal dispersion so that the resulting SC is relatively coherent over its entire bandwidth. To optimize our channel waveguides for this purpose, we carried out numerous finite-element-method simulations by varying the transverse dimensions W and H of the waveguide core. The resulting GVD curves are shown in Figs. 2 and 3 for the pump wavelengths near 1.55 μm and 3.1 μm, respectively. Note that we plot the parameter D related to the GVD parameter β_2 as $D = -(2\pi c/\lambda^2)\beta_2$. The values of W and H are chosen to ensure that D is negative (normal GVD, $\beta_2 > 0$) over a wide spectral range around the chosen pump wavelength (vertical dotted line). Notice how all GVD curves are lying below the $D = 0$ line, indicating normal dispersion over a wide wavelength range around the pump wavelength.

The GVD curves shown in Fig. 2 are for channel waveguide geometries employing a polymer for the upper cladding and silica glass for the lower cladding. To make the GVD curve peak close to 1.55 μm, thickness (H) of the waveguide is kept constant and its width (W) is varied as shown in Figs. 2(a) and 2(d). It can be observed from these figures that the peak of the GVD curves move from left to right if we increase W keeping H constant. Further, the peak value moves closer to zero as H is increased from 450 to 480 nm. In the other two sets of GVD curves shown in Figs. 2(b) and 2(c), H is varied while keeping W constant. In both cases, the peak of the GVD curves shifts upward with increasing H. As seen in Fig 2(b), $|D|$ can be made quite small at peak of the GVD curve designed to be near the pump wavelength by adjusting W and H.

The GVD curves shown in Figs. 3(a) and 3(b) assume

that the bottom cladding layer of the waveguide is made of $Ge_{11.5}As_{24}S_{64.5}$ glass. The GVD curves in Fig. 3(c) and 3(d) assume that this layer is made of MgF_2 glass. For both cases air is used as an upper cladding. It can be observed from Figs. 3(a) and 3(b) that the peak moves downward if we increase the width W while keeping thickness H constant, or decrease H while keeping W constant. In contrast, it can be observed from Fig. 3(c) that the GVD peak moves upward with increasing H at a fixed W. Notice also that the GVD peak in Fig. 3(c) occurs to the left of the pump wavelength. Finally, Fig. 3(d) shows three optimized waveguide structures when both W and H are adjusted simultaneously such that the GVD values change little for all three designs. In all cases, the pump wavelength is set at 3.1 μm (vertical dashed line).

IV. Numerical Results

The simulations of SC generation in our optimized channel waveguides were carried out by solving the Eq. (1) with the split-step Fourier method [3] after including dispersion terms up to 10^{th} order. By considering the lowest damage threshold of ChG material, we optimized our waveguide geometries for mid-infrared region SC generation in such way that the largest peak power of pump pulses is at most 3 kW. The loss parameter α of the ChG material at pump wavelengths of 1.55 μm and 3.1 μm are taken to be 3.2 dB/cm and 0.5 dB/cm, respectively [15]. The Kerr parameter n_2 is 8.6×10^{-18} m^2/W at 1.55 μm [16]. It was reduced by a factor of two at 3.1 μm. We use A_{eff} at a pump wavelength to calculate γ as the constant γ obtains a better fit between simulation and measurement than A_{eff} dependent n_2 which is described in [5]. In numerical simulations, in the case of 1.55 μm pump, we consider sech-shape input pulses of 50-fs duration with peak powers between 25 W and 100 W. However, in the case of 3.1 μm pump, pulses have 85-fs and much larger peak powers between 0.1 kW and 3 kW. These numbers are chosen to match the experiment situation [20].

A. Pumping at 1.55 μm

Based on our dispersion engineering in Fig. 2, we consider two waveguides of the same width (W = 750 nm) but two different heights (H = 480 and 450 nm). Using the finite-element mode solver, A_{eff} for these structures is found to be 0.29 μm^2 and 0.28 μm^2, respectively, and the corresponding dispersion is $D = -20$ ps/nm/km and -85 ps/nm/km. Figure 4(a) shows the SC spectra at the waveguide output at a peak power of only 25 W of 50-fs input pulses. As seen there, a relatively flat SC spectrum covering the wavelength range 1275–1975 nm (bandwidth 700 nm) could be generated with the structure for both waveguides. The SC for the waveguide with H = 480 nm exhibits a dip around the pump wavelength that does not occur for the waveguide with H = 450 nm, resulting in an ultraflat SC spectrum covering the wavelength range 1300–1900 nm for this waveguide.

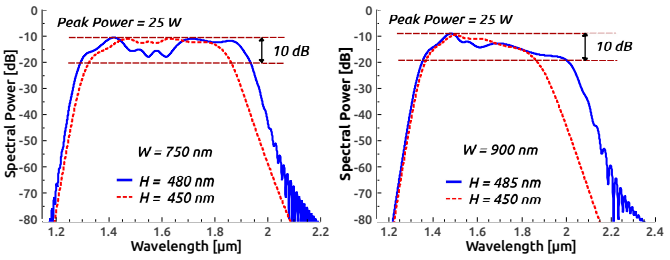

(a) (b)

Fig. 4: SC spectra of 1-cm-long ChG waveguides (core dimensions as indicated) pumped at 1.55 μm using 50-fs pulses with 25-W peak power.

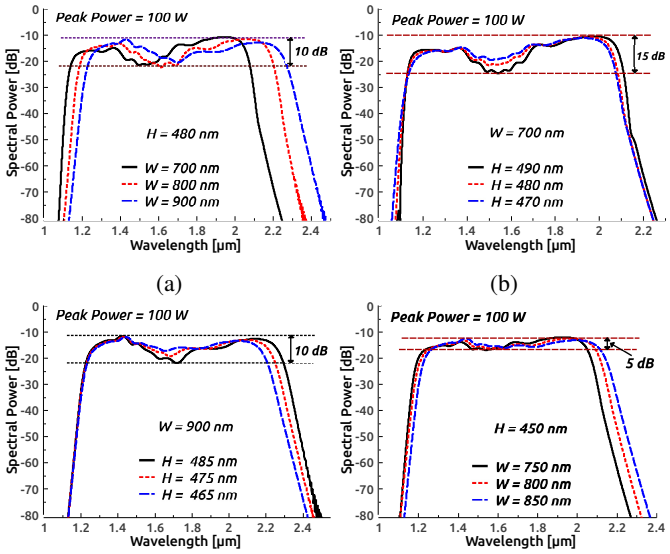

(a) (b)

(c) (d)

Fig. 5: SC spectra of 1-cm-long ChG waveguides (core dimensions as indicated) pumped at 1.55 μm using 50-fs pulses with 100-W peak power. Four figures correspond to the four set of dispersion curves in Fig. 2.

One may ask what happens if we change the width of these two waveguides while keeping nearly the same height. Figure 4(b) shows the SC spectra under identical operating conditions except that the waveguide is now wider with W = 900 nm. The dispersion parameter of the wider waveguides increases considerably and has values $D = -79$ ps/nm/km and -134 ps/km/nm for H = 450 and 485 nm, respectively. This results in an SC spectrum that is considerably asymmetric around the pump wavelength compared to the spectra in Figure 4(a). The spectrum extends over 755 nm for H = 485 nm but this bandwidth reduces to 625 nm for H = 450 nm. The main conclusions are that (i) the SC generation depends considerably on the exact values of W and H and (ii) an ultraflat SC spectrum can be obtained by optimizing waveguide dimensions even at a relatively low peak power level of only 25 W.

To study the impact of peak power of input pulses, we show four sets of SC spectra in Fig. 5 by increasing it from 25 to 100 W. These spectra correspond to the device dimensions and dispersion curves given in Fig. 2. It can be seen from Fig. 5(a) that SC spectra shift from left to right, just as the GVD curves do in Fig. 2(a). The SC bandwidth depends on the core di-

mensions and is the largest (1100 nm covering the wavelength range 1200–2300 nm) for the waveguide with $W = 900$ nm and $H = 480$ nm. Spectral density varies across the SC bandwidth but the magnitude of such variations is limited to below 10 dB in Fig. 5(a). In the second set of spectra shown in Fig. 5(b), spectral density variations increase to 15 dB, but the SC spectra do not change much as H is varied from 470 to 490 nm. The third set of SC spectra shown in Fig. 5(c) are obtained for wider waveguides. The SC bandwidth is about 1100 nm with power variations of at most 10 dB across the entire bandwidth. The best results are obtained for the fourth set of GVD curves shown in Fig. 2(d). The SC spectra in Fig. 5(d) are ultraflat with power variations of less than 5 dB across their entire bandwidth (about 900 nm). Such high-quality SC spectra are possible because our waveguides are designed to produce normal dispersion over a wide wavelength range.

B. Pumping at 3.1 μm

To extend the SC spectra into the mid-infrared range, it is necessary to increase the pump wavelength from 1.55 to 3.1 μm as seen in Fig. 3, dispersion engineering can provide us with suitable waveguide dimensions. The optimum values of both W and H are considerably larger compared to those used in Fig. 5 where pumping was at 1.55 μm. Also the material used for the two claddings are different at λ_p = 3.1 μm. We assume that air acts a upper cladding and the lower cladding is made of either $Ge_{11.5}As_{24}S_{64.5}$ glass or MgF_2 glass.

Figure 6 compares the SC spectra obtained for the two waveguides whose bottom cladding is made using these two materials. In each case, the core dimensions are optimized suitably. The core dimensions are W = 4.0 μm and H = 1.45 μm in Fig. 6(a) and W = 4.0 μm and H = 0.79 μm in Fig. 6(b). The effective mode areas for these structures are found to be 4.03 μm^2 and 2.44 μm^2, respectively. The corresponding values of GVD at the pump wavelength of 3.1 μm are $D = -5.2$ ps/nm/km and -3.9 ps/nm/km, respectively. Figure 6(a) and 6(b) show the numerical results for the two waveguides. In Fig. 6(a) the SC extends from 2 to 5.5 μm at the highest peak power of 3 kW. However, when MgF_2 glass is used for the bottom cladding, the SC is much wider in Fig. 6(b)

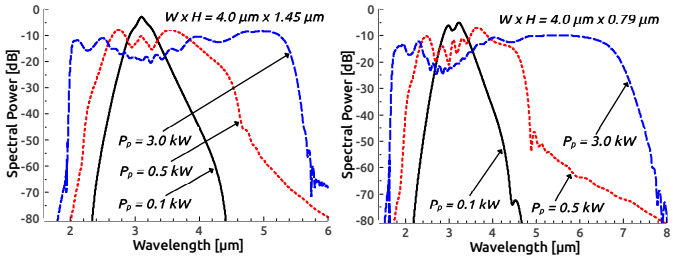

(a) (b)

Fig. 6: SC spectra of 1-cm-long ChG waveguides (core dimensions as indicated) pumped at 3.1 μm using 85-fs pulses with peak powers from 0.1-3 kW. The lower cladding of the waveguide is made of GeAsS glass in (a) and MgF_2 glass in (b).

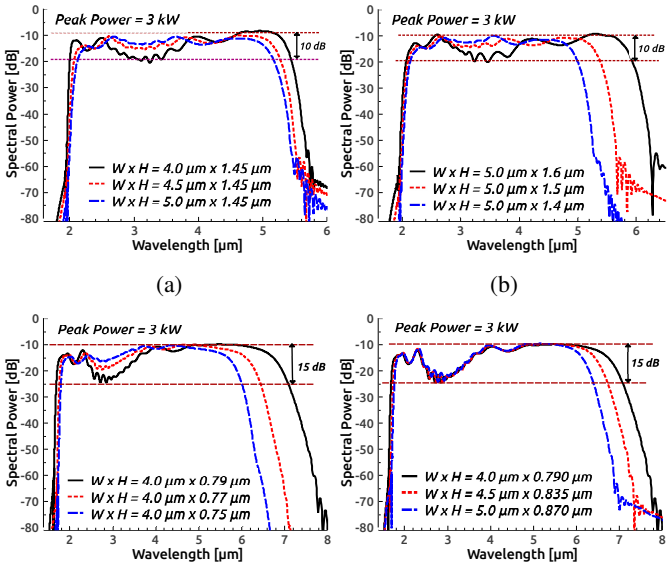

(a) (b)

(c) (d)

Fig. 7: SC spectra of 1-cm-long ChG waveguides (core dimensions as indicated) pumped at 3.1 μm using 85-fs pulses with 3 kW peak power. Four figures correspond to the four set of dispersion curves in Fig. 3.

and extends from 1.7 to 7.2 μm under the same operating conditions. These results clearly show that the use of MgF_2 glass for the bottom cladding provides better performance.

The important question is how much SC bandwidth changes if W and H are varied. To answer this question, we calculate SC spectra for all structures whose dispersion curves are shown in Fig. 3. A comparison of curves in the top and bottom rows shows that the SC is generally wider when MgF_2 glass is used for the bottom cladding of the waveguide. However, it is relatively flatter in the case of the GeAsS glass. The black curve in Fig. 7(b) that an SC spectrum spanning from 2 to 6 μm can be realized with only 10-dB variations over the entire spectral range by using the GeAsS glass for the bottom cladding. In case of a waveguide with the MgF_2-glass cladding, the SC can be widened to cover the range 1.8-7.5 μm as shown in Fig. 7(c)(solid black curve) but its flatness is somewhat reduced.

It can be seen from Fig. 7 that spectral variations can be reduced, or flatness of spectrum can be enhanced, by varying the transverse dimensions of ChG waveguides. For both structures, spectral variations can be reduced by increasing the width W while keeping the height H the same, as seen in Fig. 7(a). Spectral flatness can also be increased by reducing H while keeping W constant, as seen in Figs. 7(b) and 7(c). An ultraflat SC spectrum covering the wavelength range 2-5.5 μm is achieved for a waveguide designed with W = 5.0 μm, H = 1.5 μm and employing GeAsS for its lower cladding (dotted red curve in Fig. 7b). Similarly, an ultraflat SC spanning the wavelength range 1.8-6 μm can also be realized using a waveguide with W = 4.0 μm, H = 0.75 μm and employing MgF_2 for its lower cladding (dashed blue curve in Fig. 7(c)). In both cases, spectral variations are reduced to less than 5 dB

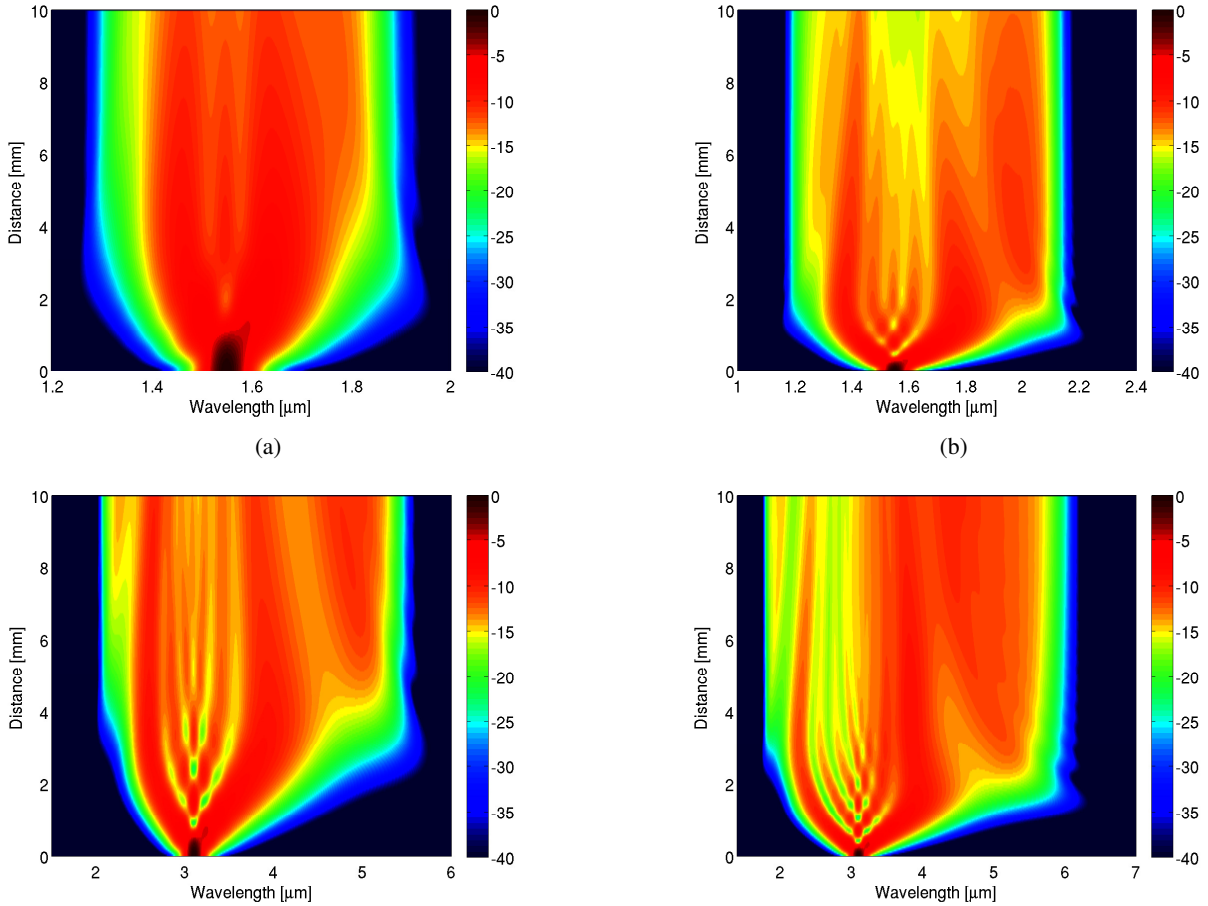

Fig. 8: Spectral evolution along a 1-cm-long waveguide with core dimensions of (a) W = 750 nm, H = 450 nm, (b) W = 800 nm, H = 450 nm, (c) W = 5 μm, H = 1.5 μm, and (d) W = 4 μm, H = 0.75 μm. The bottom cladding layer is made of silica in (a) and (b), GeAsS in (c), and MgF_2 in (d). Pump pulses are at 1.55 μm with the peak power (a) 25 and (b) 100 W and at 3.1 μm with a peak power of 3 kW (bottom row).

over the entire SC bandwidth. Our results show that, to achieve a smooth SC spectrum with reduced spectral variations, the peak of the GVD curves needs to be far below the $D = 0$ line in Fig. 3, so that the GVD is both normal and large at the pump wavelength. However, the SC bandwidth is also reduced under such conditions.

To show how the SC evolves along the waveguide length, we plot in Fig. 8, the evolution of pulse spectra over the entire waveguide length of 1-cm. As the pump lies in the normal GVD regime, SC generation is dominated initially by the self-phase modulation (SPM) process and later by the optical wave breaking process [2]. When an ultrashort optical pulse propagates in the normal-dispersion regime of a waveguide, initially its spectrum broadens symmetrically around the pump wavelength (owing to SPM). Later, longer wavelengths start to propagate faster than the shorter wavelengths, which causes the overlap of different frequency components. The temporal overlap of two spectral components leads to generation of new frequency components, resulting in side lobes on both sides of the of input spectrum (owing to optical wave breaking) that are clearly seen in Fig. 8.

V. Concluding Remarks

We have shown numerically that a 1-cm-long, dispersion-engineered, ChG planar waveguide can generate coherent, ultraflat, SC spectra in the mid-infrared region if the device is designed suitably such that it exhibits normal dispersion over a wide wavelength range around the pump wavelength. We considered pumping with femtosecond pulses at wavelengths of 1.55 and 3.1 μm, and in each case optimized the waveguide dimensions to realize a realistic dispersion profile. When such a waveguide was pumped at 1.55 μm using pulses with a peak power of only 25 W, a relatively flat SC could be generated with a bandwidth of 600 nm covering the wavelength range 1300–1900 nm. By increasing the peak power to 100 W, SC spectra could be extended to 2200 nm and had a bandwidth close to 1000 nm. Moreover, power variations were below 5 dB over the entire SC bandwidth for our optimized design.

To extend the SC spectrum further into the mid-infrared region, pump source must be shifted from 1.55 μm to longer wavelengths. Using 85-fs pump pulses with 3-kW peak power at a wavelength of 3.1 μm, we realized an ultraflat SC spectrum (spectral intensity variations of less than 5 dB) over

a wavelength range extending from 2 to 5.5 μm (>1 octave). Moreover, the spectral range could be extended from 1.8 to 6 μm if the lower cladding is made using MgF_2 glass in place of the GeAsS glass. Even a larger spectral range spanning a wavelength range from 1.7 to 7.2 μm (>2 octave) is possible when MgF_2 glass is used, but the spectral flatness is reduced considerably (up to 15 dB power variations over the entire spectral range).

Our numerical results show that ChG planar waveguides as short as 1 cm can be designed to produce good-quality SC spectra with relatively high spectral flatness. Our work may lead to new experimental activity in the important area of mid-infrared region supercontinuum generation. Such wideband coherent sources are needed for a variety of applications.

REFERENCES

[1] J. M. Dudley, G. Genty, and S. Coen, "Supercontinuum generation in photonic crystal fiber," *Rev. Mod. Phys.*, vol. 78, no. 4, pp. 1135–1184, Dec. 2006.

[2] C. Finot, B. Kibler, L. Provost, and S. Wabnitz, "Beneficial impact of wave-breaking for coherent continuum formation in normally dispersive nonlinear fibers," *J. Opt. Soc. Am. B*, vol. 25, no. 11, pp. 1938–1337, Nov. 2008.

[3] G. P. Agrawal, *Nonlinear Fiber Optics*, 5th ed. (Academic, Elsevier, 2013).

[4] A. M. Heidt "Pulse preserving flat-top supercontinuum generation in all-normal dispersion photonic crystal fibers," *J. Opt. Soc. Am. B*, vol. 27, no. 3, pp. 550–559, Mar. 2010.

[5] A. M. Heidt, A. Hartung, G. W. Bosman, P. Krok, E. G. Rohwer, H. Schwoerer, and H. Bartelt, "Coherent octave spanning near-infrared and visible supercontinuum generation in all-normal dispersion photonic crystal fibers," *Opt. Exp.*, vol. 19, no. 4, pp. 3775–3778, Feb. 2011.

[6] A. Hartung, A. M. Heidt, and H. Bartelt, "Design of all-normal dispersion microstructured optical fibers for pulse-preserving supercontinuum generation," *Opt. Exp.,* vol. 19, no. 8, pp. 7742-7749, 2011.

[7] L. E. Hooper, P.J. Mosley, A. C. Muir, W. J. Wadsworth, and J. C. Knight, "Coherent supercontinuum generation in photonic crystal fiber with all-normal group velocity dispersion," *Opt. Exp.*, vol. 19, no. 6, pp. 4902–4907, Mar. 2011.

[8] G. Stepniewski, M. Klimczak, H. Bookey, B. Siwicki, D. Pysz, R. Stepien, A. K. Kar, A. J. Waddie, M. R. Taghizadeh, and R. Buczynski, "Broadband supercontinuum generation in normal dispersion all-solid photonic crystal fiber pumped near 1300 nm," *Laser Phys. Lett.*, vol. 11, pp. 055103, Mar. 2014.

[9] B. Siwicki, M. klimczak, R. Stepien, and R. Buczynski, "Supercontinuum generation enhancement in all-solid all-normal dispersion soft glass photonic crystal fiber pumped at 1550 nm," *Opt. Fiber Tech.*, vol. 25, pp. 64–71, Oct. 2015.

[10] Z. Guo, J. Yuan, C. Yu, X. Sang, K. Wang, B. Yan, L. Li, S. Kang, and X. Kang, "Highly coherent supercontinuum generation in the normal dispersion liquid-core photonic crystal fiber," *Prog. in Elec. Res.*, vol. 48, pp. 67–76, May. 2016.

[11] C. Wei, X. Zhu, R. A. Norwood, F. Seng, and N. Peyghambarian, "Numerical investigation on high power mid-infrared supercontinuum fiber lasers pumped at 3 μm," *Opt. Exp.*, vol. 21, no. 24, pp. 29488–29504, 2013.

[12] B. J. Eggleton, B. Luther-Davies, and K. Richardson, "Chalcogenide photonics," *Nat. Photonics*, vol. 5, pp. 141–148, 2011.

[13] L. Liu, T. Cheng, K. Nagasaka, H. Tong, G. Qin, T. Suzuki, and Y. Ohishi, "Coherent mid-infrared supercontinuum generation in all-solid chalcogenide microstructured fibers with all-normal dispersion," *Opt. Lett.*, vol. 41, no. 2, pp. 392–395, Jan. 2016.

[14] A. Al-Kadry, L. Li, M. E. Amraoui, T. North, Y. Messaddeq, and M. Rochette, "Broadband supercontinuum generation in all-normal dispersion chalcogenide nanowires," *Opt. Lett.*, vol. 40, no. 20, pp. 4687–4690, Oct. 2015.

[15] P. Ma, D. Y. Choi, Y. Yu, X. Gai, Z. Yang, S. Debbarma, S. Madden, and B. Luther-Davies, "Low-loss chalcogenide waveguides for chemical sensing in the mid-infrared," *Opt. Exp.*, vol. 21, no. 24, pp. 29927–29937, Dec. 2013.

[16] Y. Yu, B. Zhang, X. Gai, P. Ma, D. Choi, Z. Yang, R. Wang, S. Debbarma, S. J. Madden, and B. Luther-Davies, "A broadband, quasi-continuous, mid-infrared supercontinuum generated in a chalcogenide glass waveguide," *Laser Photonics Rev.*, pp. 1–7, 2014.

[17] Y. Yu, X. Gai, P. Ma, K. Vu, Z. Yang, R. Wang, D. Choi, S. Madden, and B. Luther-Davies, "Experimental demonstration of linearly polarized 210 m supercontinuum generation in a chalcogenide rib waveguide," *Opt. Lett.*, vol. 41, no. 5, pp. 958-961, Mar. 2016.

[18] M. R. Karim, B. M. A. Rahman, and G. P. Agrawal, "Dispersion engineered $Ge_{11.5}As_{24}Se_{64.5}$ nanowire for supercontinuum generation: A parametric study," *Opt. Exp.*, vol. 22, no. 25, pp. 31029–31040, Dec. 2014.

[19] M. R. Karim, B. M. A. Rahman, and G. P. Agrawal, "Mid-infrared supercontinuum generation using dispersion-engineered $Ge_{11.5}As_{24}Se_{64.5}$ chalcogenide channel waveguide," *Opt. Exp.*, vol. 23, no. 5, pp. 6903–6914, Mar. 2015.

[20] F. Silva, D. R. Austin, A. Thai, M. Baudisch, M. Hemmer, D. Faccio, A. Couairon, and J. Biegert, "Multi-octave supercontinuum generation from mid-infrared filamentation in a bulk crystal" *Nat. Commun.*, vol. 3, no. 807, pp. 1–5, 2012.

[21] B. M. A. Rahman and J. B. Davies, "Finite-element solution of integrated optical waveguides," *J. Lightwave Technol.*, vol. 2, pp. 682–688, Oct. 1984.